J Appl Electrochem (2011) 41:307–315
DOI 10.1007/s10800-010-0240-5

ORIGINAL PAPER

Effect of aluminium microstructure on corrosion and inhibiting effect of polyacrylic acid in H_2SO_4 solution

S. A. Umoren · Y. Li · F. H. Wang

Received: 15 February 2010 / Accepted: 24 October 2010 / Published online: 17 November 2010

Abstract The corrosion behaviour of a microcrystalline aluminium (mc-Al) coating fabricated from pure cast aluminium substrate by magnetron sputtering and the pure polycrystalline aluminium (pc-Al) were studied using electrochemical impedance spectroscopy and potentiodynamic polarization techniques in aerated 0.5 M H_2SO_4 at 30 ± 1 °C. The corrosion inhibiting effect of polyacrylic acid (PAA) and synergistic effect of iodide ions was also investigated. Results obtained show that surface microcrystallization increases the corrosion susceptibility of pure cast aluminium leading to decrease in interfacial impedance and an increase in the kinetics of the anodic dissolution. Introduction of PAA into the corrosive medium was observed to retard the corrosion rates of both specimens. The inhibition mechanism was affected by the microstructure of the sample. PAA functions as a mixed inhibitor but under cathodic control for pc-Al and under anodic control for mc-Al. Addition of iodide ions synergistically increased the inhibition efficiency of PAA and this effect was more pronounced with mc-Al.

Keywords Microcrystallization · Aluminium · Polyacrylic acid · Corrosion inhibition · Synergism

S. A. Umoren · Y. Li (✉) · F. H. Wang
State Key Laboratory for Corrosion and Protection, Institute of Metal Research, Chinese Academy of Sciences, 62 Wencui Road, Shenyang 110016, People's Republic of China
e-mail: liying@imr.ac.cn

S. A. Umoren
Department of Chemistry, Faculty of Science, University of Uyo, P.M.B 1017 Uyo, Nigeria

1 Introduction

Increasing cost and inaccessibility of less active metals has led to the use of active metals in most industrial applications. One of the major problems of such metals is their susceptibility to corrosion when exposed to aggressive environments. Significant measures have been taken to increase the corrosion resistance of these base metals which amongst them include reducing the impurity content of the metals, incorporation of suitable alloying element as well as surface modification approach.

Nowadays, microcrystallization/nanocrystallization has become a useful means of improving materials performance particularly in corrosion protection applications. This is often attributed to their small grain sizes (1–100 nm for nanocrystalline and 100–1000 nm for microcrystalline materials) and high volume fraction of grain boundaries [1, 2] giving rise to unique physical, chemical and mechanical properties compared to their polycrystalline counterparts. Reports on the corrosion performance of microcrystalline/nanocrystalline materials can be found in the literature though with varying results depending on the nature of material and environment. For instance, Li et al. [3] reported that the corrosion rate of surface nanocrystallized low carbon steel in acid sulphate solution was higher than that of bulk steel. Ye et al. [4] found that a significant improvement in corrosion resistance was noted for nanocrystallized 309 stainless steel in NaCl solution, no noteworthy influence was observed in Na_2SO_4 solution. Also, Liu et al. [5] reported that nanocrystallization significantly increased the resistance of Ni-based superalloy to pitting corrosion in 0.5 M NaCl + 0.05 M H_2SO_4 and attributed the low pitting corrosion resistance of the cast alloy in NaCl acidic solution to its heterogeneous microstructure. Similarly, it was found that corrosion resistance of

microcrystalline Al (mc-Al) coating deteriorated more compared to that of cast pure Al in Na_2SO_4 acidic solution while its oxide film has higher pitting resistance in NaCl acidic solution [6].

The protection of these metals can be achieved in multiple ways among which the treatment of the corrosive medium is one of the most important ones [7]. A suitable method in this regard is the introduction of suitable inhibitors into the corrosive medium to retard the corrosion reaction and reduce corrosion rate. Polymers have been found to be suitable for this purpose and their inhibiting action is widely attributed to their adsorption onto the metal surface through the heteroatoms (N and O) of their functional groups which serves as adsorption centres [8–11].

Some studies have been carried out on the corrosion inhibition of aluminium and its alloy in different aqueous environments, but no reports exist to our knowledge on corrosion inhibition of their microcrystalline or nanocrystalline counterparts. However, a little information is available on corrosion inhibition of nanocrystalline iron and mild steel as well as synergistic effect of corrosion inhibiting additives on nanocrystalline structures. Oguzie et al. [12] investigated the corrosion inhibiting effect of methionine and synergistic effect of KI additives on nanocrystalline low carbon steel fabricated from low carbon steel substrate by magnetic sputtering technique. Results obtained indicate that surface nanocrystalliztion increases the corrosion susceptibility of low carbon steel leading to a decrease in interfacial impedance and an increase in the kinetics of the anodic reaction. Methionine was found to inhibit the corrosion of both surface nanocrystallized low carbon steel (SNCLCS) and the bulk low carbon steel (BLCS) with comparable inhibition efficiencies and iodide ions synergistically increased the inhibition efficiency that was more pronounced on the BLCS. Cysteine has been reported to function as a corrosion inhibitor for both nanocrystalline (BNII) and polycrystalline (CPII) iron samples in 0.5 M H_2SO_4. It was found to be strictly a cathodic inhibitor for CPII and a mixed type inhibitor for BNII. Addition of iodide ions increased the protective efficiency of cysteine but the inhibition mechanism was found to remain unaffected [13]. In a related study, the corrosion and corrosion inhibition of bulk nanocrystalline ingot iron (BNII) fabricated from conventional polycrystalline ingot iron (CPII) by severe rolling technique in 0.1 M H_2SO_4 by thiourea (TU) and influence of iodide ions has been reported [14]. It was found that BNII was more susceptible to corrosion in the uninhibited solution. The presence of TU improved corrosion resistance of both iron samples comparably; however, addition of KI diminished the inhibition performance of TU by chemically modifying the nature of the interfacial species responsible for the inhibiting effect.

To extend the investigation to other service conditions, we studied the corrosion and corrosion inhibition effect of mc-Al in acidic medium using a polymer as inhibitor as well as the effect of iodide ion additives. This is the first report on mc-Al, using a polymer as an inhibitor. The suitability of polyacrylic acid (PAA) as a corrosion inhibitor for aluminium has been established in earlier reports [15].

2 Experimental

The test specimens were polycrystalline pure cast aluminium (pc-Al) (99.99%) and mc-Al coating. The mc-Al coated on quartz glass substrate was fabricated from the polycrystalline pure cast aluminium by magnetron sputtering technique. The details of the magnetron sputtering technique and subsequent characterization of the microstructure of mc-Al have been described in previous reports [6, 16]. The pc-Al was machined into test coupons of dimension 1 cm × 1 cm which were wet polished with silicon carbide abrasive paper (from # 400 to # 2000), degreased in absolute ethanol, rinsed with distilled water and dried in warm air.

The corrosive medium was 0.5 M H_2SO_4 prepared from analytical reagent grade concentrated acid using distilled water. The test inhibitor was PAA. Two different concentrations 2×10^{-3} and 1×10^{-4} M were prepared using 0.5 M H_2SO_4 and used in the study. 0.5 and 5 mM KI were introduced into the inhibited solution (2×10^{-3} M PAA) to assess the effect of iodide ions additives.

Electrochemical measurements were carried out in all the test solutions using both dc (potentiodynamic polarization) and ac (EIS) techniques. Electrochemical experiments were performed using a PARC Parstat-2273 Advanced Electrochemical System operated with Powercorr and Powersine software. For all experiments, a conventional three-electrode glass cell was used with platinum foil as counter electrode and saturated calomel electrode (SCE) as the reference electrode which was connected via Luggin's capillary. All the potentials reported are with reference to SCE. All experiments were undertaken in stagnant aerated conditions at 30 ± 1 °C. The working electrode was immersed in a test solution for 30 min or until a stable open circuit potential was attained. Potentiodynamic polarization measurements were carried out in a potential range of ±250 mV vs. corrosion potential (E_{corr}) at a scan rate of 0.5 mV s^{-1}. Electrochemical impedance spectroscopy (EIS) studies were made at corrosion potentials (E_{corr}) over a frequency range of 100 kHz to 10 mHz with a signal amplitude perturbation of 5 mV. Analyses of the spectra were performed using Zsimpwin software also supplied by PARC.

3 Results and discussion

3.1 Specimens microstructures

The X-ray diffraction (XRD) patterns of the surface layers of pc-Al and mc-Al are depicted in Fig. 1a and b, respectively. As could be observed from the figure, the positions of the diffraction peaks remain the same indicating that composition of the two specimens were the same and that the lattice parameters were not affected by surface microcrystallization and moreso, no new phases were formed. However, there is evidence of slight broadening of the diffraction peaks of the mc-Al specimen. A similar observation has been reported by other authors [3, 12] and was attributed to crystalline imperfections induced by the small grain size and microstrain. Figure 2 shows the SEM micrographs for (a) pc-Al and (b) mc-Al surfaces. The pc-Al surface is characterized by a relatively homogeneous coarse-grained microtopography compared to that of mc-Al. The magnified image of mc-Al surface shown in Fig. 3 allows a clear visualization of the sub micro morphology and the thickness of the mc-Al coating which was about 5 μm. Previous report [6] indicated the average grain size of the coating was about 400 nm.

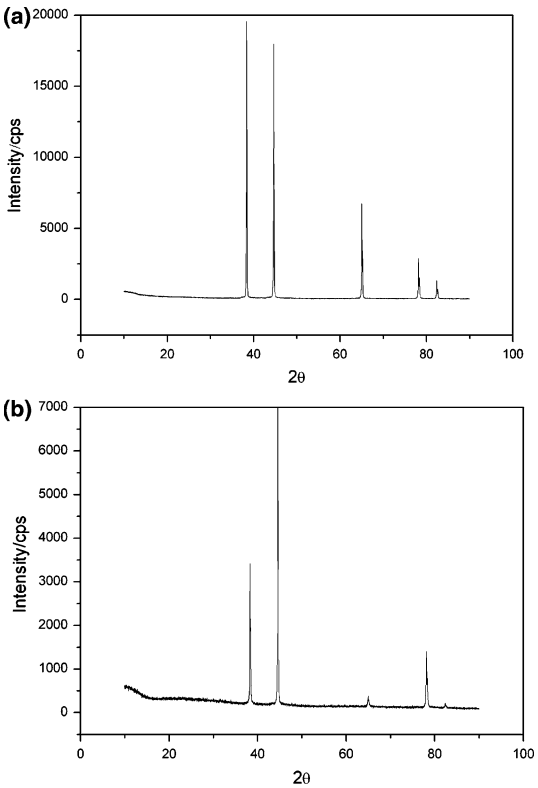

Fig. 1 XRD patterns of **a** pc-Al and **b** mc-Al

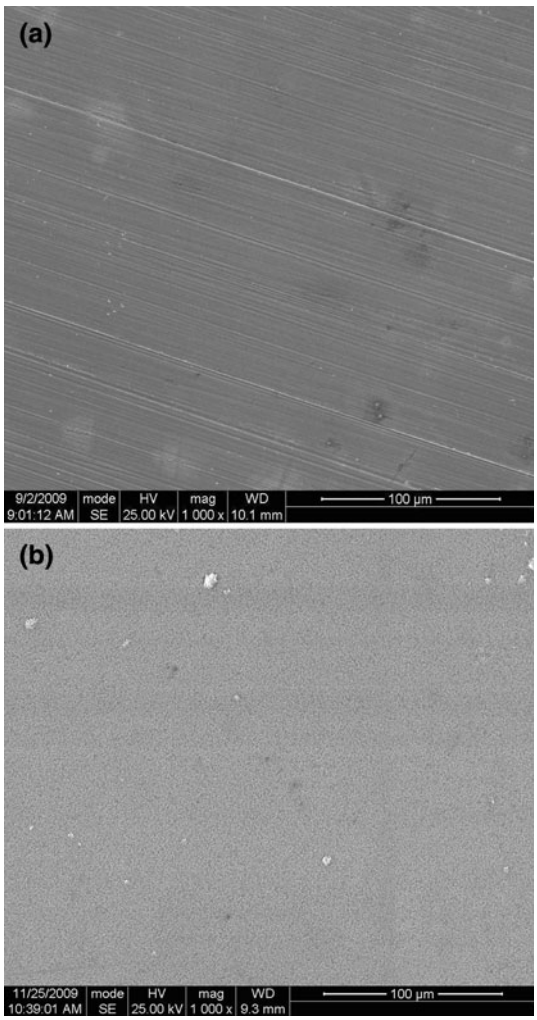

Fig. 2 SEM micrographs of **a** pc-Al and **b** mc-Al

3.2 Electrochemical corrosion behaviour of mc-Al and pc-Al in uninhibited acid

3.2.1 EIS measurements

The impedance behaviour is well suited for determining the characteristics and kinetics of electrochemical processes occurring at mc-Al/0.5 M H_2SO_4 and pc-Al/0.5 M H_2SO_4 interfaces. The impedance plots for both mc-Al and pc-Al in 0.5 M H_2SO_4 are illustrated as Nyquist and Bode plots in Fig. 4a and b, respectively. It is observed that the plots for the two specimens are identical indicating the same corrosion characteristics. However, the decrease in the size of the semicircle for mc-Al compared to pc-Al indicates that mc-Al is more susceptible to corrosion in the acidic environment. The Nquist plots are characterized by three time constants consisting a large capacitive loop at high frequencies (HF), an inductive loop at medium frequencies (MF) followed by the second capacitive loop at low

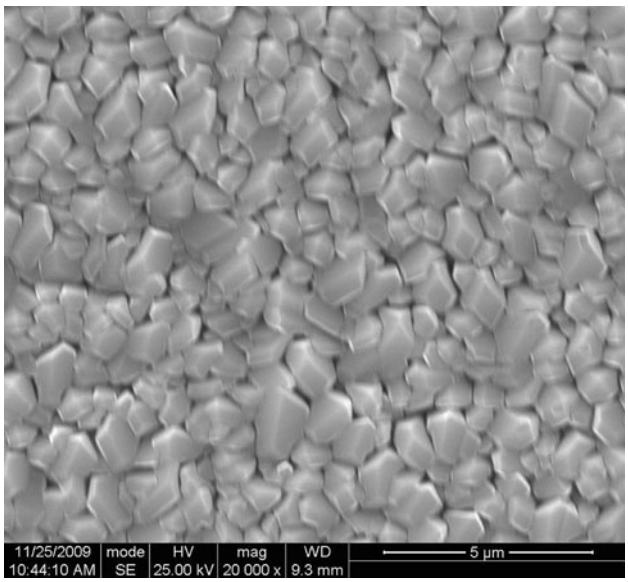

Fig. 3 High magnification of SFM micrographs of mc-Al

frequencies (LF). There has been no general agreement in the literature regarding the origin of time constants found in the impedance diagram. The high frequency capacitive loop could be attributed to the relaxation process in the aluminium oxide (or hydrated oxide) film present on the aluminium surface and its dielectric properties [15, 17, 18] since the oxide film is considered to be a parallel circuit of a resistor due to the ionic conduction of the oxide film and a capacitor due to its dielectric properties [18]. Another possible explanation for the origin of the capacitive loop at high frequency as put forward by Brett [19] and reported in [20] is the reactions involved in the formation of the oxide layer. Brett suggested that at the metal–oxide interface aluminium is oxidized to Al^{+} intermediates. The Al^{+} intermediates will subsequently be oxidized to Al^{3+} at the oxide–solution interface where also O^{2-} or OH^{-} is formed. At the same time with the formation of O^{2-} ions, H^{+} ions are formed. Consequently, this results in a local acidification at the oxide–electrolyte interface. The electrode impedance in this case was determined by the metal/oxide interface, the oxide film and the oxide/solution interface [17]. The inductive loop observed at MF may be attributed to bulk or surface relaxation of species in the oxide [21]. Adsorption of intermediates (H^{+} and SO_4^{2-} ions) could also cause an inductive loop. The second capacitive loop observed at LF could be assigned to the metal dissolution [15].

The impedance data was analyzed using the equivalent circuit (EC) model shown in Fig. 5. The model includes the solution resistance, R_s, a series combination of a film resistance R_f, inductance L in parallel with inductance resistance R_L, double layer capacitance C_{dl} in parallel with charge transfer resistance R_{ct} and the constant phase

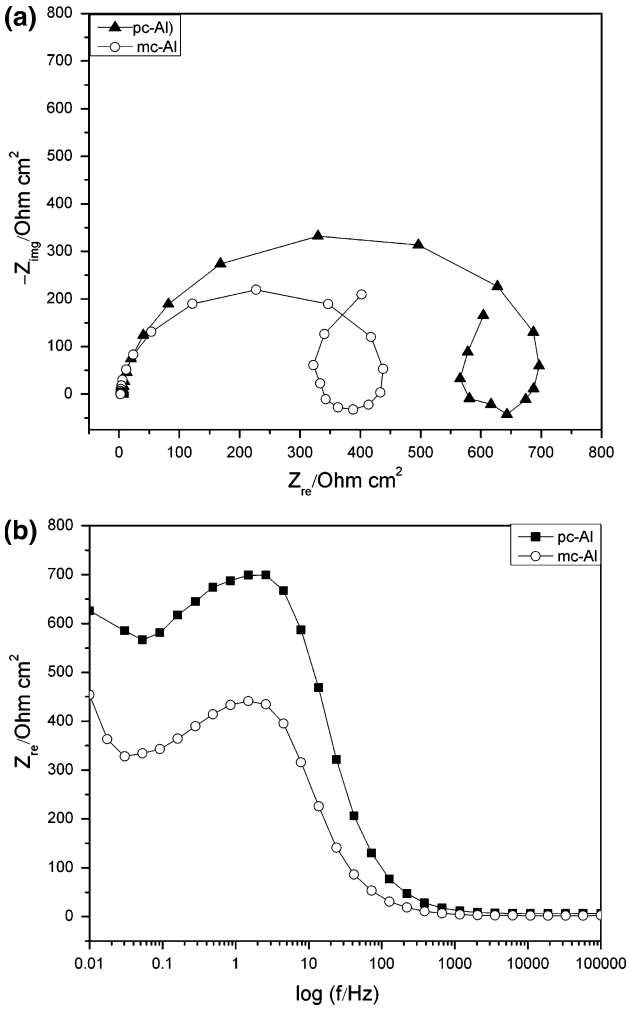

Fig. 4 Nyquist **a** and Bode **b** plots of pc-Al and mc-Al in 0.5 M H_2SO_4 in the absence of inhibitor (PAA)

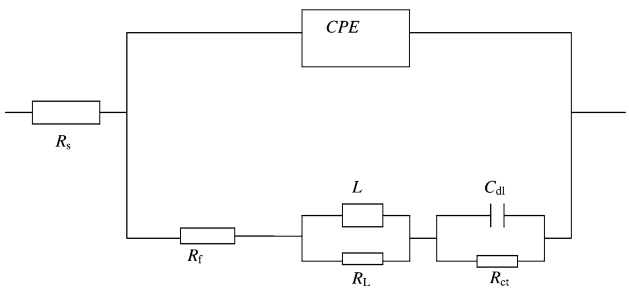

Fig. 5 The electrochemical equivalent circuit used for simulation of impedance spectra

element, CPE. The CPE defined by the values of Y_o and n is used in place of a capacitor to compensate for deviations from ideal dielectric behaviour associated with the non-homogeneity of the electrode surface. The impedance of CPE is given by:

$$Z_{\mathrm{CPE}} = \frac{1}{(Y_{\mathrm{o}} j\omega)^n} \quad (1)$$

where j is an imaginary number and ω is the angular frequency in rad s^{-1}, $\omega = 2\pi f$ and f is the frequency in Hz.

The fitting Nyquist plots deduced from the experimental and simulated data (not shown), show that the fitting results are in good agreements with the experimental data. In accordance with EC, the polarization resistance R_p is given as:

$$R_p = R_f + R_L + R_{ct} \quad (2)$$

The electrochemical impedance parameters obtained for both samples are listed in Table 1. The charge transfer resistance of mc-Al and pc-Al as shown in the table are 733 and 1119 Ω cm^2, respectively, while the respective polarization resistances are 1186 and 1557 Ω cm^2. The lower charge transfer resistance and polarization resistance for mc-Al indicate that it is more vulnerable to corrosion in the acidic medium.

3.2.2 *Potentiodynamic polarization measurements*

Potentiodynamic polarization reactions were undertaken to distinguish the effect of surface microcrystallization on the anodic and cathodic corrosion reactions in 0.5 M H_2SO_4. Typical potentiondynamic curves for the two specimens are illustrated in Fig. 6. It is seen in the figure that both specimens underwent active dissolution with no distinctive passivation up to about 1.0 V vs. SCE. Similar observation has been reported by Zhang et al. [6] for the same materials in 0.5 M Na_2SO_4 solution. The similarity of the polarization curves could suggests that similar corrosion mechanism should be applicable for both specimens. However, it is obvious that surface microcrystallization impacted negatively on the polarization behaviour of pure cast aluminium in 0.5 M H_2SO_4. As could be seen from the polarization parameters listed in Table 1, the corrosion potential (E_{corr}) was lowered from −759 mV for pc-Al to −971 mV for mc-Al while the corrosion current density (i_{corr}) increased from 75 to 93 μA cm^{-2}. The lower E_{corr} and higher i_{corr} of the mc-Al coating indicate that its anodic reaction was promoted and cathodic reaction (hydrogen evolution) was inhibited hence higher corrosion susceptibility of the mc-Al specimen. Oguzie et al. [12] and Li et al. [3] have reported similar behaviour for nanocrystalline low carbon steel surface produced by magnetron sputtering and ultrasonic shot peening respectively in acid sulphate solution.

The XRD results indicate identical composition for mc-Al and pc-Al, it is therefore pertinent to say that the differences in corrosion behaviour is mainly due to the differences in grain size and the ensuing surface structural modification. The microcrystalline surface with mean grain size in micrometre scale provides both high population active sites and greater surface area (Fig. 3) for the corrosion reaction. In addition, the considerable volume of grain boundaries enhances the diffusion of the corrodent within the surface [12]. These factors could be responsible for the observed high dissolution kinetics of mc-Al compared to pc-Al. As could also be rightly observed in Fig. 6, the effect of microcrystallization was more pronounced on the anodic dissolution reaction and cathodic reaction was less affected. As pointed out by Li et al. [3], this suggests a predominant influence of the number of active sites, which could accelerate the kinetics of the anodic reaction by forming several micro-electrochemical cells. In a related study by Jung and Alfantazi [22], they observed identical anodic polarization behaviour for nano and micro Co in 0.1 M H_2SO_4, whereas the cathodic kinetics of the nano increased. The increase in the cathodic kinetics was attributed to increased hydrogen evolution reaction rate due to substantial quantity of crystalline defects in the nanocrystalline electrode.

Table 1 Electrochemical impedance parameters for mc-Al and pc-Al in 0.5 M H_2SO_4 without and with inhibitors

System/concentration	R_{ct} (Ω cm^2)	C_{dl} (mF cm^{-2})	R_p (Ω cm^2)	η%
mc-Al				
Blank (0.5 M H_2SO_4)	733	114	1186	–
1×10^{-4} M PAA	499	97	1190	03
2×10^{-3} M PAA	1892	41	2884	58
2×10^{-3} M PAA + 0.5 mM KI	2864	39	3400	65
2×10^{-3} M PAA + 5 mM KI	5856	24	7364	84
pc-Al				
Blank (0.5 M H_2SO_4)	1119	83	1557	–
1×10^{-4} M PAA	731	62	1589	02
2×10^{-3} M PAA	1094	47	1978	21
2×10^{-3} M PAA + 0.5 mM KI	1266	40	2205	29
2×10^{-3} M PAA + 5 mM KI	1675	38	2715	43

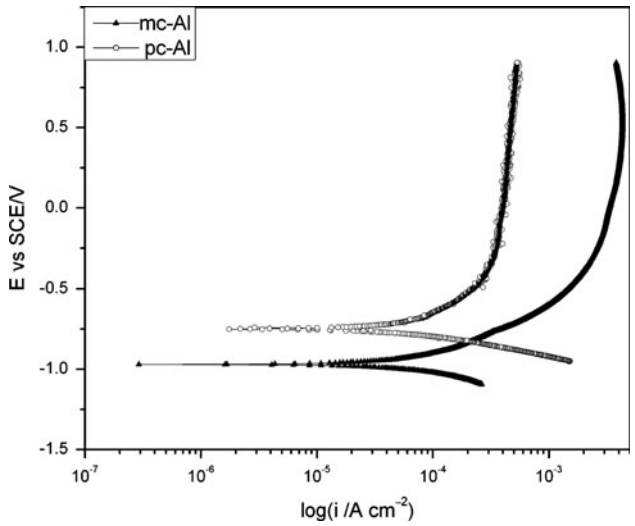

Fig. 6 Polarization curves of pc-Al and mc-Al in 0.5 M H_2SO_4 in the absence of inhibitor (PAA)

3.3 Electrochemical corrosion behaviour of mc-Al and pc-Al in inhibited acid

3.3.1 EIS measurements

Figure 7 shows the impedance behaviour as exemplified in Nyquist plots for (a) pc-Al and (b) mc-Al in 0.5 M H_2SO_4 in the absence and presence of 1×10^{-4} and 2×10^{-3} M PAA. It could be observed from the figure that the shape of the impedance diagrams increases but not altered on addition of PAA, suggesting that similar mechanisms for the metal dissolution in 0.5 M H_2SO_4 occurred in the absence and presence of the additive. The observed increase in the size of the semicircles of the Nyquist plots on introduction of PAA to the corrosive medium for both samples is associated with corrosion inhibiting effect of PAA. The Nyquist plots are also characterized by three time constants consisting two capacitive loops at high and low frequencies and an inductive loop at medium frequencies. The inductor arises from adsorption effects of the oxide film and/or PAA molecules and could be defined as ($L = R\tau$), where τ is the relaxation time for adsorption on the aluminium surface [20]. The depressed form of the higher frequency loop reflects the surface inhomogeneity of structural or interfacial origin such as those found in adsorption processes [23, 24]. The same EC shown in Fig. 5 was used to fit the experimental data and the corresponding impedance parameters are listed in Table 1. The marked increase in the impedance parameters especially with increase in concentration of PAA for both pc-Al and mc-Al is attributed to corrosion inhibiting effect of the additive. R_p values increase from 1557 to 1978 Ω cm^2 for pc-Al and from 733 to 1892 Ω cm^2 for mc-Al at the highest concentration (2×10^{-3} M) of PAA investigated. Also the corresponding values of C_{dl} reduced from 83 to 47 mF cm^{-2} and 114 to 41 mF cm^{-2} for pc-Al and mc-Al, respectively. The decrease in double layer capacitance on the introduction of PAA to the acid solution may indicate the presence of a protective layer that covers the surface of the electrode. The decrease in C_{dl} is in accordance with Helmholtz model given by the following equation [25]:

$$C_{dl} = \frac{\varepsilon\varepsilon_0 A}{d} \tag{3}$$

where d is the thickness of the protective layer, ε is the dielectric constant of the medium, ε_0 is the vacuum permittivity and A is the effective area of the electrode. A quantitative measure of the protective ability of PAA for the two specimens can be obtained by comparing the values of polarization resistance in the absence and presence of the inhibitor as follows [26]:

$$\eta\% = \left(1 - \frac{R_p^{-1}}{R_p^{0-1}}\right) \times 100 \tag{4}$$

where R_p^o and R_p are the polarization resistances in the absence and presence of inhibitor (PAA), respectively. The values of inhibition efficiency obtained were 21 and 58% for pc-Al and mc-Al, respectively, at 2×10^{-3} M PAA concentration, which clearly shows that the microcrystalline structure of mc-Al provides a more favourable surface for PAA adsorption.

Experiments were also undertaken to assess the effects of Al microstructures on the efficiency of PAA (2×10^{-3} M) in the presence of iodide ions. The impedance spectra of (a) pc-Al and (b) mc-Al in 0.5 M H_2SO_4 containing 2×10^{-3} M PAA in combination with 0.5 and 5 mM KI and PAA alone for comparison are shown in Fig. 8. The Nyquist plots again revealed that the impedance responses of the two Al specimens do not differ significantly without and with iodide ions. The Nyquist plots were characterized by three time constants and the size of the diameter of the semicircles increases on introduction of iodide ions compared to PAA alone and further increased with increase in iodide ion concentration for both mc- Al and pc-Al. The same EC in Fig. 5 was used to analyze the impedance spectra and the corresponding data are given in Table 1. Addition of iodide ions resulted in significance increase in R_{ct}, R_p and $\eta\%$ and decrease in C_{dl} values which could be attributed to synergistic effect. The effect was more pronounced for mc-Al compared to pc-Al. For instance in the presence of 5 mM KI, the $\eta\%$ increased from 58 to 84% for mc-Al compared to an increase from 21 to 43% for pc-Al.

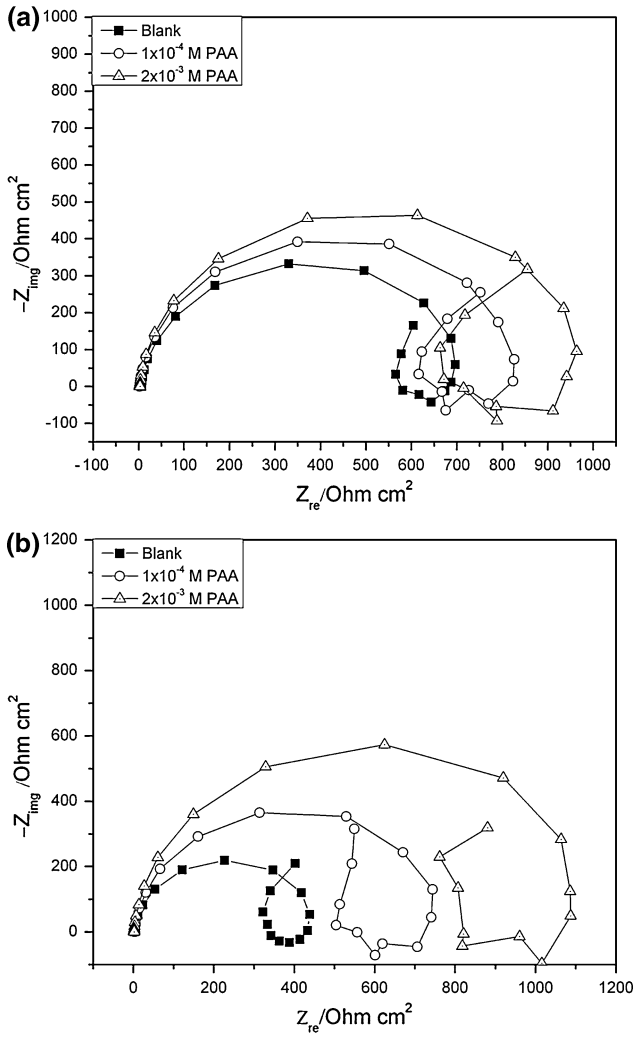

Fig. 7 Nyquist plots of **a** pc-Al and **b** mc-Al in 0.5 M H_2SO_4 in the absence and presence of different concentration of PAA

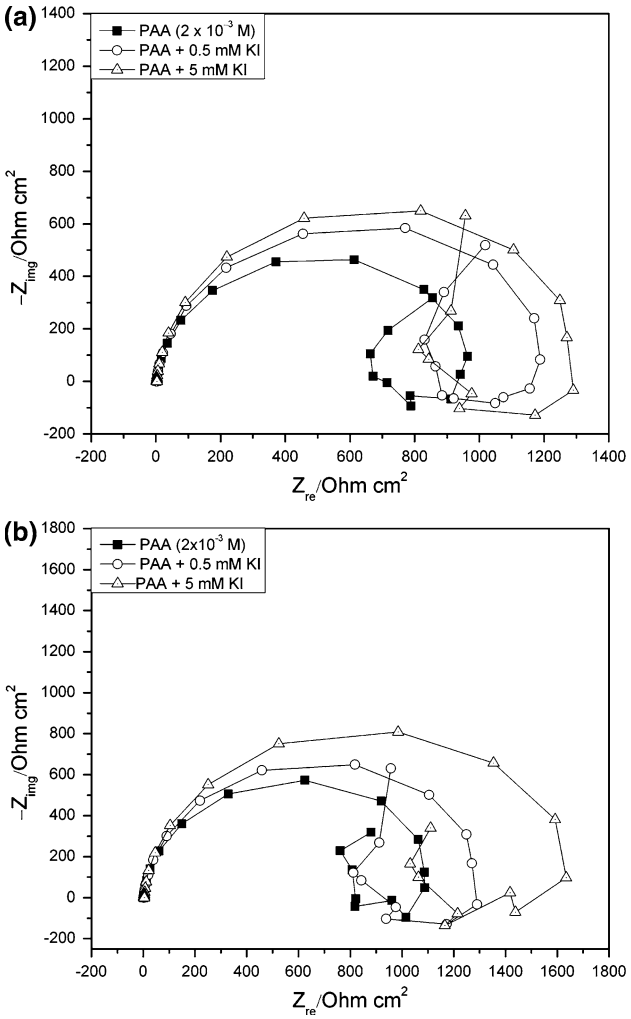

Fig. 8 Nyquist plots of **a** pc-Al and **b** mc-Al in 0.5 M H_2SO_4 in the presence of 2×10^{-3} M PAA and in combination with different concentrations of KI

3.3.2 Potentiodynamic polarization measurements

Potentiodynamic polarization studies were carried out to distinguish the effect of microcrystallization on the anodic and cathodic corrosion reactions in 0.5 M H_2SO_4 containing the different concentrations of PAA. Typical anodic and cathodic polarization curves for the specimens in acidic solution containing the test inhibitor are illustrated in Fig. 9a for pc-Al and Fig. 9b for mc-Al and the electrochemical parameters are given in Table 2. As could be observed from the plots and table, introduction of PAA into the corrosive solution, shifts the corrosion potential to the anodic direction incase of mc-Al and slightly shifted to the cathodic direction for pc-Al sample. However, both the anodic (β_a) and cathodic (β_c) Tafel slopes are affected which seems to suggest that PAA functions as a mixed inhibitor but under anodic and cathdoic control for mc-Al and pc-Al, respectively. A quantitative measure of the protective effect using polarization measurements can be obtained by comparing the values of the corrosion current densities in the absence (i^o_{corr}) and presence of inhibitor (i_{corr}) as follows:

$$\eta\% = \left(1 - \frac{i_{corr}}{i^o_{corr}}\right) \times 100 \quad (5)$$

Inhibition efficiency values for mc-Al and pc-Al in the acid solution containing the different concentrations of PAA are listed in Table 2. The results presented in the table show that PAA at lower concentration (1×10^{-4} M) stimulated the corrosion of both specimens (−33 and −44% for mc-Al and pc-Al, respectively) and an inhibiting effect at higher concentration (26 and 23 for mc-Al and pc-Al, respectively). These values are low compared to the ones obtained by EIS measurements although the same trend is followed. Similar observation has been reported by

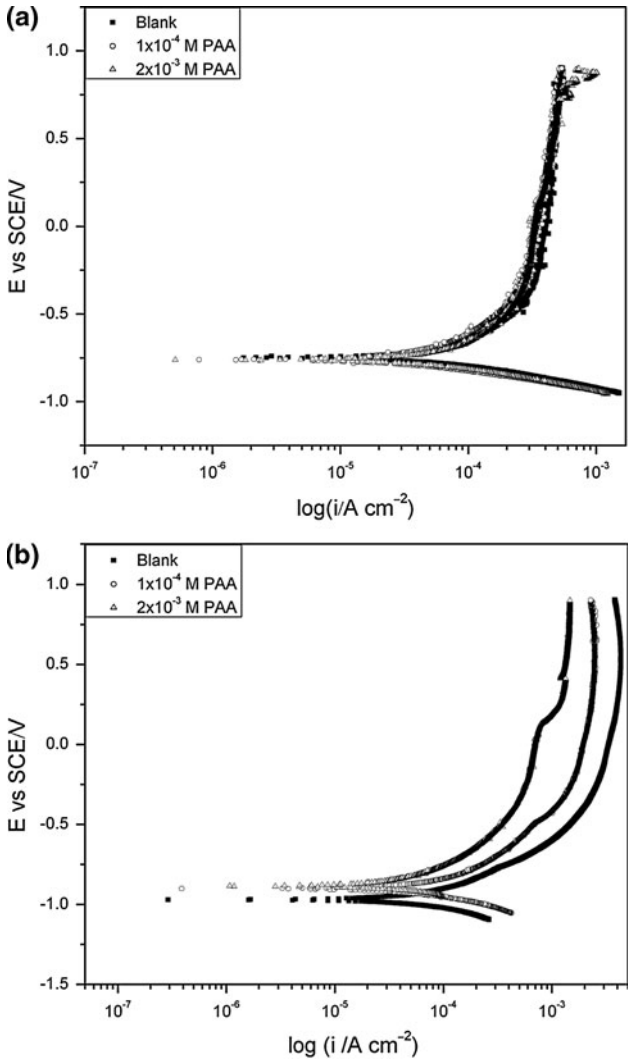

Fig. 9 Polarization curves of **a** pc-Al and **b** mc-Al in 0.5 M H_2SO_4 in the absence and presence of different concentration of PAA

Oguzie et al. [13] for bulk nanocrystalline (BNII) and coarse polycrystalline (CPII) ingot iron in 0.5 M H_2SO_4 containing cystein as inhibitor. The lower values of $\eta\%$ from polarization technique according to Oguzie et al. [13] could be attributed to predominant influence of the anodic dissolution process in determining the corrosion rate.

The polarization curves obtained when 0.5 and 5 mM KI were added to 2×10^{-3} M PAA in 0.5 M H_2SO_4 are illustrated in Fig. 10 for (a) pc-Al and (b) mc-Al. As could be observed from the plots, addition of KI shifts the corrosion potential to less noble values with more pronounced effect at lower KI concentration in both specimens. This implies that the inhibitor in the presence of KI affects the cathodic reaction more than the anodic reaction, suggesting that the hydrogen evolution reaction is retarded. The synergistic effect between PAA and KI in retarding the corrosion of pc-Al and mc-Al is again apparent from the corresponding electrochemical parameters displayed in Table 2 with more pronounced effect noted for mc-Al. For example, the inhibition efficiency ($\eta\%$) increased from 26 to 72% on addition of 5 mM KI to 2×10^{-3} M PAA for mc-Al compared to an increase from 23 to 59% for pc-Al. The mechanism of this synergistic effect has been described in detail in the literature [27–29]. The iodide ions are strongly chemisorbed on the corroding Al surface and facilitate PAA adsorption by acting as intermediate bridges between the positively charged metal surface and PAA polycation. This stabilizes the adsorption of PAA on the Al surface, leading to higher surface coverage. Again the differences in the results for the corrosion behaviour of the two aluminium samples in the presence of PAA alone and on addition of iodide ions could be attributed to their differences in microstructure. Results obtained in this study and earlier studies [12] have shown that microcrystalline/

Table 2 Polarization parameters for mc-Al and pc-Al in 0.5 M H_2SO_4 without and with inhibitors

System/concentration	E_{corr} (mV/SCE)	i_{corr} (μA cm^{-2})	βc (mV dec^{-1})	βa (mV dec^{-1})	$\eta\%$
mc-Al					
Blank (0.5 M H_2SO_4)	−971	93	196	397	–
1×10^{-4} M PAA	−900	124	221	734	−33
2×10^{-3} M PAA	−885	69	314	761	26
2×10^{-3} M PAA + 0.5 mM KI	−994	51	197	346	45
2×10^{-3} M PAA + 5 mM KI	−965	26	169	392	72
pc-Al					
Blank (0.5 M H_2SO_4)	−759	75	177	455	–
1×10^{-4} M PAA	−760	108	217	1453	−44
2×10^{-3} M PAA	−763	58	138	426	23
2×10^{-3} M PAA + 0.5 mM KI	−779	42	105	238	44
2×10^{-3} M PAA + 5 mM KI	−784	31	131	365	59

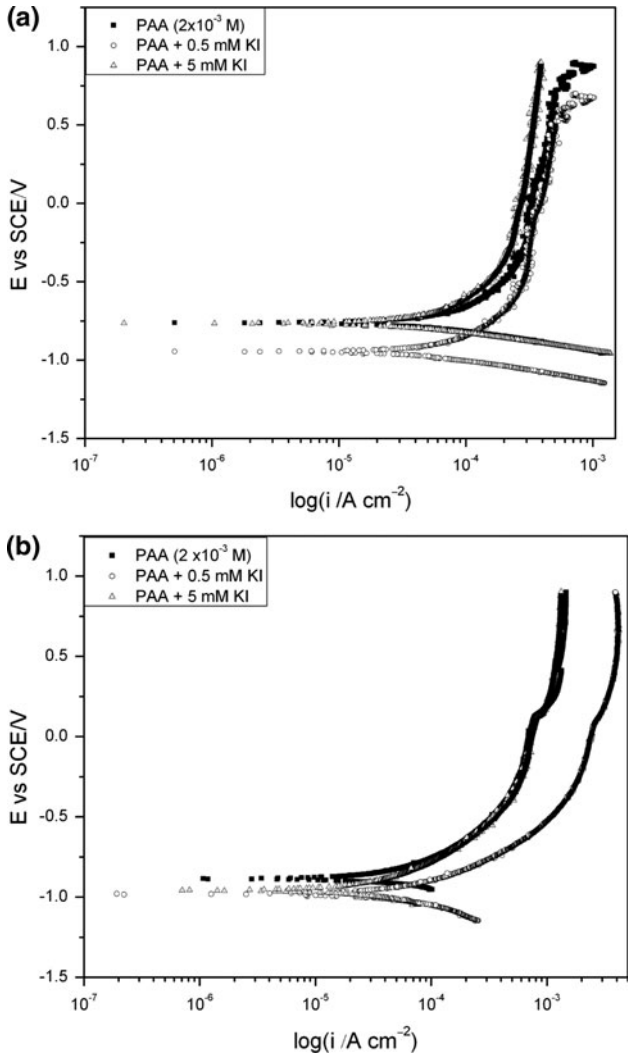

Fig. 10 Polarization curves of **a** pc-Al and **b** mc-Al in 0.5 M H_2SO_4 in the presence of 2×10^{-3} M PAA and in combination with different concentrations of KI

nanocrystalline surface favours inhibitor adsorption. This could imply that the high defect population (grain boundaries, triple junctions, inclusions) which promotes metal dissolution also provides an abundance of receptor sites for the inhibitor.

4 Conclusions

The electrochemical corrosion and inhibition by PAA of mc-Al in 0.5 M H_2SO_4 has been compared with that of pure pc-Al. The mc-Al coating was fabricated from the polycrystalline pure cast aluminium by magnetron sputtering technique. EIS and potentiodynamic polarization studies indicate that both specimens have identical corrosion mechanism in 0.5 M H_2SO_4 solution. The results, however, show that the micrograined microstructure accelerated the corrosion aluminium in acidic medium by shifting the corrosion potential to the negative values and increasing the kinetics of the anodic reaction. PAA functions as a corrosion inhibitor for both pc-Al and mc-Al aluminium sample, exerting a greater inhibiting effect on the latter. The inhibition mechanism was affected by the microstructure of the sample. For pc-Al, PAA functions as a mixed inhibitor but under cathodic control, whereas for mc-Al it was under anodic control. Addition of iodide ions synergistically increased the inhibition efficiency of PAA and this effect was more pronounced with mc-Al.

Acknowledgments S.A. Umoren acknowledges the Chinese Academy of Sciences (CAS) and Academy of Sciences for the Developing World (TWAS) for the CAS-TWAS Postdoctoral Fellowship

References

1. Klabunde JL (ed) (2001) Nanoscale materials in chemistry. John Wiley & Sons Inc., New York
2. Liu D, Wang F, Cao Ch (1990) Corrosion 46:975
3. Li Y, Wang F, Liu G (2004) Corrosion 60:891
4. Ye W, Li Y, Wang F (2006) Electrochim Acta 51:4426
5. Liu L, Li Y, Wang F (2007) Electrochim Acta 52:2392
6. Zhang B, Li Y, Wang F (2007) Corros Sci 49:2071
7. Shen CB, Wang SG, Yang HY, Long K, Wang FH (2006) Appl Surf Sci 253:2118
8. Ashassi-Sorkhabi H, Ghalebsaz-Jeddi N, Hashemzadeh F, Jahani H (2006) Electrochim Acta 51:3848
9. Aly KI, Wahdan MH, Hussein MA (2009) J Appl Polym Sci 112:513
10. Umoren SA, Ogbobe O, Ebenso EE, Okafor PC (2007) J Appl Polym Sci 105:3363
11. Benabdellah M, Ousslim A, Hammouti B, Elidrissi A, Aouniti A, Dafali A, Bekkouch K, Benkaddour M (2007) J Appl Electrochem 37:819
12. Oguzie EE, Li Y, Wang FH (2007) Electrochim Acta 52:6988
13. Oguzie EE, Li Y, Wang FH (2007) J Solid State Electrochem 12:721
14. Oguzie EE, Li Y, Wang FH (2009) J Phys Chem C 113:8420
15. Amin MA, Abdel Rehim SS, El-Sherbini EFF, Hazzaci OA, Abbas MA (2009) Corros Sci 51:658
16. Zhang B, Li Y, Wang F (2009) Corros Sci 51:268
17. Mansfeld F, Lin S, Kim K, Shih H (1987) Corros Sci 27:997
18. Mansfeld F, Lin S, Kim K, Shih H (1988) Werkst Korros 39:487
19. Brett CMA (1990) J Appl Electrochem 20:1000
20. Khaled KF, Amin MA (2009) J Appl Electrochem 39:2553
21. Frers SE, Stefenel MM, Mayer CM, Chierchie T (1990) J Appl Electrochem 20:996
22. Jung H, Alfantazi A (2006) Electrochim Acta 51:1806
23. Gonclaves RS, Azambuja DS, Serpa Lucho AM (2002) Corros Sci 44:467
24. Zhang Q, Hua Y (2010) Mater Chem Phys 119:57
25. Khaled KF, Al-Qahtani MM (2009) Mater Chem Phys 113:150
26. Noor EA (2009) Mater Chem Phys 114:533
27. Umoren SA, Ebenso EE (2007) Mater Chem Phys 106:387
28. Umoren SA, Li Y, Wang FH (2010) Corros Sci 52:1777
29. Jeyaprabha C, Sathiyanarayanan S, Venkatachari G (2005) J Electroanal Chem 583:232